Heliyon 10 (2024) e38034

Contents lists available at ScienceDirect

Heliyon

journal homepage: www.cell.com/heliyon

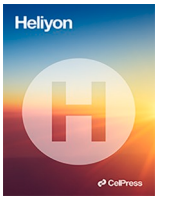

Research article

Exosomes derived from Danshen decoction-pretreated bone marrow mesenchymal stem cells alleviate myocardial infarction via anti-apoptosis and up-regulation of autophagy

Qian Yang, Qi-Ming Zhong, Mei-qing Song, Li-guo Tong, Chong-zhi Bai *

Central Laboratory, Shanxi Province Hospital of Traditional Chinese Medicine, No. 70, Nanshifang Street, Taiyuan City, Shanxi Province, 030012, China

A B S T R A C T

Cardiomyocyte loss and myocardial fibrosis are major determinants of myocardial infarction (MI) pathological changes. Mesenchymal stem cell (MSC)-derived exosomes (exos) and Danshen decoction (DSY) have been demonstrated to mediate cardiac repair following MI. BM-MSCs exos or BM-MSCsDSY exos were intramuscularly injected into post-MI rats. On the 7th, 14th and 28th days, serum CK, LDH, α-HBDH, ALT, and AST were measured and electrocardiogram changes were monitored to identify cardiac function; Triphenyltetrazolium chloride staining, Hematein&Eosin staining, Masson trichrome staining and Transmission Electron Microscope were adopted to analyze infarct area, cardiac morphology, histopathology, and fibrosis and cardiomyocyte ultrastructure; TUNEL assay, real-time PCR and western blot were performed to detect cardiomyocyte apoptosis and autophagy. As a result, BMMSCsDSY exos are superior to BM-MSCs-exos in improvement of cardiac function, morphology, histopathology and cardiomyocyte ultrastructure, as well as in reduction of infarction area and cardiac fibrosis by inhibiting apoptosis and promoting autophagy of cardiomyocytes.

1. Background

Myocardial infarction (MI), the leading cause of death and disability worldwide, is the most severe form of coronary heart disease, accounting for over a third of annual deaths in developed countries [1]. Standard clinical treatments for MI include percutaneous coronary intervention, coronary artery bypass surgery, and antithrombotic therapy [2]. While these methods can alleviate vascular stenosis and improve patient survival rates, they do not significantly reduce MI-related mortality or regenerate damaged cardiac tissue.

Mesenchymal stem cells (MSCs) originate from mesoderm and ectoderm during early embryo development and can be found in connective tissue and organ stroma. They can be obtained from various sources, including bone marrow, fat, umbilical cord, liver, and dental pulp [3]. MSCs have multi-directional differentiation capabilities, allowing them to transform into osteoblasts, chondrocytes, nerve cells, and cardiomyocytes under induced conditions [4]. It has been discovered that MSC transplantation can reduce myocardial infarction size, improve cardiac function, and alleviate adverse left ventricular remodeling, thus playing a role in MI treatment [5,6]. Furthermore, numerous studies have shown that extracellular vesicles secreted by MSCs, especially exosomes, address the low survival, differentiation, and homing rates and immune rejection of MSC transplantation [7]. Exosomes exhibit anti-cardiomyocyte apoptosis, promote angiogenesis, reduce infarct size, combat myocardial fibrosis, and accelerate cardiac recovery due to their low immunogenicity, biodegradability, toxicity, and natural encapsulation of endogenous bioactive molecules [8].

Exosomes are small extracellular vesicles ranging from 40 to 160 nm in diameter, released by various cells and playing a crucial role

* Corresponding author.
E-mail addresses: annieyang1990@163.com (Q. Yang), qmzhong@pku.org.cn (Q.-M. Zhong), smqxjy666@163.com (M.-q. Song), dboy-007@163.com (L.-g. Tong), baicz@im.ac.cn (C.-z. Bai).

https://doi.org/10.1016/j.heliyon.2024.e38034
Received 19 November 2023; Received in revised form 12 August 2024; Accepted 16 September 2024
Available online 17 September 2024

in intercellular communication [9]. The production of extracellular vesicles (EVs) depends on the cellular origin, metabolic status, and microenvironment of the cells [10]. Alterations in these factors can change the constituents enriched in exosomes, thereby inducing phenotypic and molecular alterations in recipient cells. Moreover, different modes of therapeutic exosomes uptake by recipient cells, including receptor-mediated endocytosis, involvement of clathrin-coated pits, lipid rafts, phagocytosis, caveolae structures, and micropinocytosis, can result in distinct localization, degradation, and/or functional outcomes of the exosomal constituents [11]. Exosomes can either merge with cell membranes to release their contents directly into the cytoplasm or trigger intracellular signaling through ligand-receptor interactions, thereby modulating cellular behavior indirectly. Thus, it is possible to modify the effect of exosomes on recipient cells by regulating the microenvironment or interfering with exosome uptake pathways, ultimately affecting disease progression.

Danshen decoction, a traditional Chinese medicine (TCM) treatment, is composed of Salvia miltiorrhiza (Danshen), Santali Albi Lignum (Tanxiang), and Fructus amomi (Sharen). It is commonly used to treat "different pains in the heart and abdomen" and has the ability to promote blood circulation, remove blood stasis, smooth qi and blood, and relieve pain. It is effective in treating qi stagnation, blood stasis, and stomach pain. Clinical and basic studies have confirmed that it can improve myocardial pathological changes, alleviate myocardial ultrastructural damage, and inhibit cardiomyocyte necrosis and apoptosis, exhibiting significant anti-MI efficacy. [12].

Based on this analysis, we hypothesized that pretreatment with Danshen decoction would enhance the efficacy of exosomes from bone marrow mesenchymal stem cells (BM-MSCs) against MI. In this study, we report the superior efficacy of exosomes from BM-MSCs^{DSY} compared to BM-MSCs, particularly in anti-apoptosis and pro-autophagy, as well as cardiac morphology, function, and myocardial ultrastructure recovery. These findings provide scientific evidence supporting the development of therapeutic strategies to enhance the effects of exosomes from BM-MSCs in MI treatment.

2. Methods

The study was approved by the Medical Ethics Committee of Shanxi Academy of Traditional Chinese Medicine (SZYLY2020KY-0301) and complied with the International Association of Veterinary Editors' Consensus Author Guidelines on Animal Ethics and Welfare.

2.1. Isolation and pretreatment of BM-MSCs

Sprague-Dawley (SD) rats (BEIJING HFK BIOSCIENCE Co., Ltd.) were housed in a temperature (22 ± 1 °C) and humidity (50 ± 10 %) controlled room with a 12-h light-dark cycle and had free access to water and chow. Under sterile conditions, BM-MSCs were harvested from the bone marrow of the tibia and femur in SD rats (50–60 g) and cultured in DMEM/F12 medium supplemented with 10 % fetal bovine serum and 1 % penicillin-streptomycin at 37 °C and 5 % CO_2. After 48 h, the non-adherent cells were discarded during media exchange and passaged seven to ten days later. Passage 3–4 BM-MSCs were pretreated with DMEM/F12 complete medium containing 0.16 g/L DSY aqueous extract for three days.

2.2. Extraction and identification of exosomes

Exosomes were extracted by differential centrifugation. Briefly, after BM-MSCs reached 80–85 % confluence, they were cultured in FBS-free DMEM/F12 medium for another 24 h. The conditioned supernatants of BM-MSCs pretreated with or without DSY were collected and centrifuged at 2000g for 10 min and subsequently at 12000g for 30 min at 4 °C, followed by filtration through a 0.22-μm filter to remove dead cells and cell debris. The filtrate obtained was then ultracentrifuged at 110000 g for 1 h. Then, the supernatant was removed, and the pellet was washed in a large volume of PBS and ultracentrifuged at the same speed. The exosome pellet was resuspended in PBS and stored at −80 °C for further experiments. The protein concentrations of exosomes were quantified by the MicroBCA Protein Assay Kit. The morphologies and particle sizes of exosomes were analyzed by transmission electron microscopy (TEM) and nanoparticle tracking analysis (NTA), respectively. Additionally, the exosome markers CD9 were identified by Western blot.

2.3. Establishment of MI model

Seventy-two male Sprague-Dawley (SD) rats weighing 200–250 g (BEIJING HFK BIOSCIENCE Co., Ltd.) were housed in a temperature (22 ± 1 °C) and humidity (50 ± 10 %) controlled room with a 12-h light-dark cycle and had free access to water and chow. They were randomly assigned into the sham group (n = 6), the model group (n = 6), the BM-MSCs-exos group (n-6) and the BM-MSCs^{DSY}-exos group (n = 6). Moreover, 7 d, 14 d, and 28 d post-surgery were set as the detection time points.

Male SD rats were anesthetized by intraperitoneal injection of 2 % pentobarbital sodium (10 ml/kg) and fixed on the operating table. Following endotracheal intubation in the supine position under a respiratory frequency of 80 breaths/min, a tidal volume of 4.0 ml, and a respiratory ratio of 1:1, the skin was disinfected, and the muscles were bluntly separated, then incised between the 3rd and 4th intercostal spaces. The heart was extruded, and the left anterior descending artery was ligated with a 6-0 silk suture at 0.5 mm depth and 2 mm width in the model group, while perforation instead of ligation was conducted in the sham group. Moreover, rats in the BM-MSCs-exos or BM-MSCs^{DSY}-exos group were intra-myocardially injected with 40 μg exosomes derived from BM-MSCs or BM-MSCs^{DSY}, respectively. Finally, the muscle and skin incisions were carefully sutured layer by layer, and penicillin sodium (200000U/d) was injected intramuscularly to prevent infection for three days.

2.4. Monitoring of electrocardiogram

The electrocardiograms were recorded using the BL-420S Biofunctional Experiment System. Briefly, after anesthesia, the red electrode was connected to the upper left limb, the black electrode was connected to the lower left limb, and the white electrode was connected to the right forelimb. At least 60 s of ECG signal was recorded. Analysis of ECG waves was done to calculate heart rate (beats/min), QRS complex, and J point (mV).

2.5. Determination of myocardial enzymes

Blood samples were harvested from the inferior vena cava and centrifuged at 3000 rpm for 15 min to obtain serum. The serum was stored at −20 °C for subsequent assays. The serum biochemical markers, including the activity of creatine kinase (CK), alpha-hydroxybutyrate dehydrogenase (α-HBDH), lactate dehydrogenase (LDH), alanine aminotransferase (ALT), and aspartate aminotransferase (AST), were analyzed using an automatic biochemistry analyzer (Fort, Italy).

2.6. Cardiac morphology

On the 7th, 14th, and 28th post-operative days, we observed and recorded detrimental alterations of cardiac morphology in hearts.

2.7. Measurement of myocardial infarction area

The hearts were removed, washed in PBS (pH = 7.4), frozen at −20 °C for 30 min, and then cut into 1–2 mm thickness sections perpendicularly along the long axis from apex to base. The slices were incubated with 2 % 2, 3, 5-triphenyl tetrazolium chloride (TTC) phosphate buffer (pH 7.4) at 37 °C for 15 min to visualize the infarct area. The infarcted volume was calculated using Image-J software (version 1.52a), with red indicating normal tissue and white indicating infarcted tissue.

2.8. Cardiac histopathology and fibrosis

The hearts were removed, and the infarct area and non-ischemic area were accurately separated, then fixed in 10 % buffered neutral formalin solution. Fixed samples were dehydrated in a serial ascending dilution of ethanol and xylene and then embedded in paraffin wax. Thin sections of 5 μm were cut and stained with hematoxylin and eosin (H&E) or Masson's trichrome. The slides were examined to detect the degree of pathological damage and fibrosis of cardiac tissues under a light microscope (Olympus BX51, Japan).

2.9. Myocardial cell ultrastructure

The samples were fixed in 2.5 % glutaraldehyde at 4 °C, washed three times with 0.1M PBS (pH = 7.4) (15 min for each time), fixed in 1 % osmic acid fixative for 3 h, dehydrated in ascending series of alcohol (50 %, 70 %, 90 %, and 100 %), and embedded in Epon812. The semi-thin sections were stained with 1 % toluidine blue and observed under a light microscope (Olympus BX51, Japan); ultrathin sections were collected on copper grids, stained with uranyl acetate, and examined under a transmission electron microscope (JEOL Ltd., Japan).

2.10. Observation of cardiomyocyte apoptosis

The paraffin-embedding sections were dewaxed, treated with proteinase K for 30 min, then incubated with TUNEL reaction mixtures according to the kit procedure (KeyGEN), developed with the DAB solution, stained with hematoxylin, and analyzed under a light microscope (Olympus BX51, Japan).

2.11. Quantitative real-time PCR

Total RNA in heart tissue was extracted with TRIzol reagent. 200 ng of total RNA was subjected to reverse transcription using an RT First Strand cDNA Synthesis Kit in a total volume of 20 μL under the following conditions: 25 °C for 10 min, 55 °C for 30 min, and 85 °C for 5 min. Quantitative real-time PCR (RT-qPCR) was conducted in triplicate using SYBR Green Mix under reaction conditions: 95 °C for 5 min, followed by 40 cycles of 95 °C for 10 s and 60 °C for 30 s. The specific primers used for qPCR are presented in Supplementary Table 1, and GAPDH was used as the reference gene.

2.12. Western blot analysis

The heart tissues were prepared as homogenates in precooled radioimmunoprecipitation assay (RIPA) buffer supplemented with protease and phosphatase inhibitors for 30 min on ice, and centrifuged at 15000 rpm for 30 min at 4 °C. The protein concentration was determined using the bicinchoninic acid (BCA) protein assay kit (Biosharp, Beijing, China). 50 μg of protein and 3 μl of the pre-stained molecular weight marker were separated with SDS-PAGE under the condition of concentration gel at 80 V and separation gel at 120 V and subsequently semi-dry transferred to a 0.22μm PVDF membrane (Millipore A/S, Copenhagen, Denmark) at 15 V for 55 min using a

semi-dry electroblotting system (Transblot SD; Bio-Rad). After being washed thrice with Tris-buffered saline Tween-20 (TBST) (10 min each), the membrane was blocked with 5 % nonfat dry milk in TBST at room temperature for 2 h with gentle agitation. The blocked membrane was incubated with a primary antibody (1:1000 for Bax, 1:1000 for Bcl-2, 1:500 for Cleaved Caspase-3, and 1:500 for GSK-3β) at 4 °C overnight. After being washed thrice with TBST (10 min each), the membrane was then incubated with anti-rabbit IgG-HRP secondary antibody (1:10000) at room temperature for 1 h with gentle agitation. After being washed again, the membrane was subsequently visualized with enhanced chemiluminescent (ECL) detection reagent according to the manufacturer's instructions and digitized using the FluorChem HD2 system (Alpha, USA). β-actin was selected as an internal control. Quantitative analysis of the protein bands was conducted using Image-J software.

2.13. Statistical analysis

The data are expressed as means ± SEM. Statistical analysis for multiple comparisons was performed by one-way ANOVA followed by Dunnett's post-hoc test using GraphPad Prism software (version 6.0). Pearson's correlation analysis was employed for normally distributed data, while Spearman's correlation analysis was employed for non-normally distributed data. A P value < 0.05 was considered statistically significant.

3. Results

3.1. Isolation and identification of exosomes from BM-MSCs

After 24 h of incubation for cell adherent growth, BM-MSCs displayed a fibroblast-like shape and fish-school-like distribution, with typical MSC characteristics. The exosomes were 30–150 nm in diameter, with an average particle size of 75.73 nm. Exosome marker CD9 was positively expressed in BM-MSCs exos and BM-MSCs^{DSY} exos, as detected by Western Blot analysis (Fig. 1).

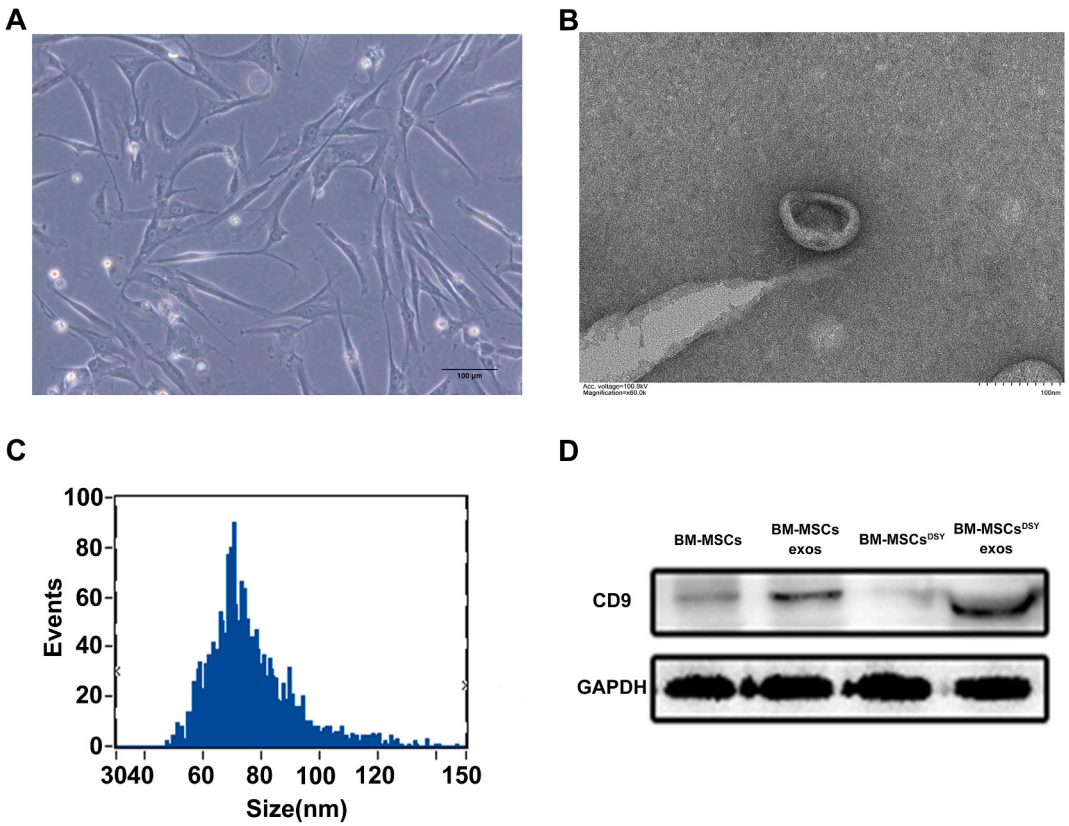

Fig. 1. Isolation and identification of exosomes derived from BM-MSCs A. The morphology of BM-MSCs was characterized as being spindle-shaped under a light microscope (× 200); B. The morphology of BM-MSCs exos was identified by a transmission electron microscope (× 60000); C. The count and size distribution of BM-MSCs exos was detected by Nanoparticle tracking analysis (NTA); D. The exosomal marker protein CD9 was confirmed by Western blot.

3.2. BM-MSCs^{DSY} exos preserved post-MI cardiac function

3.2.1. Serum myocardial zymogram alterations

Compared to the model group, serum expression levels of CK, LDH, α-HBDH, ALT, and AST increased on the 7th, 14th, and 28th days following myocardial injection of BM-MSCs exos or BM-MSCs^{DSY} exos (Fig. 2A–E). Specifically, α-HBDH and ALT levels in the sham group, α-HBDH levels in the BM-MSCs exos group, and LDH, α-HBDH, and AST levels in the BM-MSCs^{DSY} exos group were significantly increased ($P < 0.01$) on the 7th day. Furthermore, LDH levels in the BM-MSCs exos group and CK, LDH, α-HBDH, ALT, and AST levels in the BM-MSCs^{DSY} exos group were significantly increased ($P < 0.01$) on the 28th day.

3.2.2. Electrocardiogram changes

In the sham group, QRS wave and T-wave appeared normal, and the J-point remained at baseline. In contrast, the model group displayed elevated J-points and T-wave amplitudes on the 7th day, with significant increases on the 14th and 28th days. Additionally, the model group exhibited a nearly equal increase in Q- and R-wave amplitudes on the 14th day and a larger increase in Q-wave amplitude than R-wave amplitude on the 28th day. Compared to the model group at each time point, J-points in the BM-MSCs exos group and the BM-MSCs^{DSY} exos group were significantly decreased ($P < 0.01$). See Fig. 2F–G for details.

3.3. BM-MSCs^{DSY} exos improved post-MI cardiac morphology, histopathology and cardiomyocyte ultrastructure

3.3.1. Variation in myocardial infarct size and fibrosis

No infarct size was observed in the sham group. However, the model group exhibited increased infarct size, left ventricular dilation, and wall thinning with prolonged observation time. Compared to the model group, both BM-MSCs exos and BM-MSCs^{DSY} exos significantly reduced infarct size ($P < 0.01$ on the 14th day and $P < 0.05$ on the 28th day in the BM-MSCs exos group; $P < 0.01$ on the 14th and 28th days in the BM-MSCs^{DSY} exos group). See Fig. 3A–B for details.

Additionally, collagen fiber expression gradually increased with prolonged observation time in the model group. In comparison, no proliferation was observed in the sham group, while slighter degrees of proliferation were found in the BM-MSCs exos and BM-MSCs^{DSY} exos groups. See Fig. 3C for details.

3.3.2. Morphological changes in heart size and shape

As shown in Fig. 3D, the forearm and apical segments of the left ventricular myocardium appeared normal in the sham group on the 7th, 14th, and 28th days. In the model group, the myocardium was pale and the left ventricle hypertrophied on the 7th day, followed by aggravated damage on the 14th day and dark myocardium with heart atrophy on the 28th day. In the BM-MSCs exos group, the myocardium was purple and heart shape was relatively normal on the 7th day, while the myocardium was slightly pale on the 14th day and gray with heart atrophy on the 28th day. In the BM-MSCs^{DSY} exos group, the myocardium was reddish-purple on the 7th day and slightly pale on the 14th and 28th days, with no significant changes in heart shape at any observation time.

3.3.3. Histopathological changes in the heart

In the sham group, myocardial fibers were regularly arranged with clear striations, cardiomyocytes were intact, and inflammatory

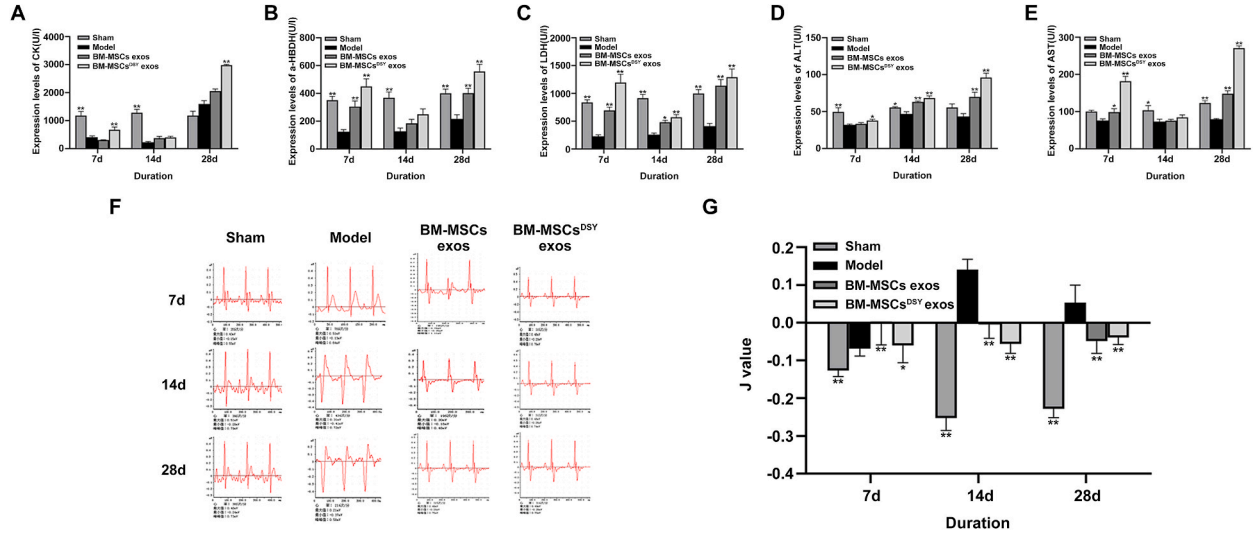

Fig. 2. Intramuscular injection of BM-MSCs^{DSY} exos can improve post-MI cardiac function A-E. The CK, LDH, α-HBDH, ALT, and AST levels in serum on the 7th, 14th, and 28th days after MI; F-G. Cardiac function was evaluated by electrocardiogram. Data are presented as Mean ± SEM, n = 6, $^{**}P < 0.01$, $^{*}P < 0.05$.

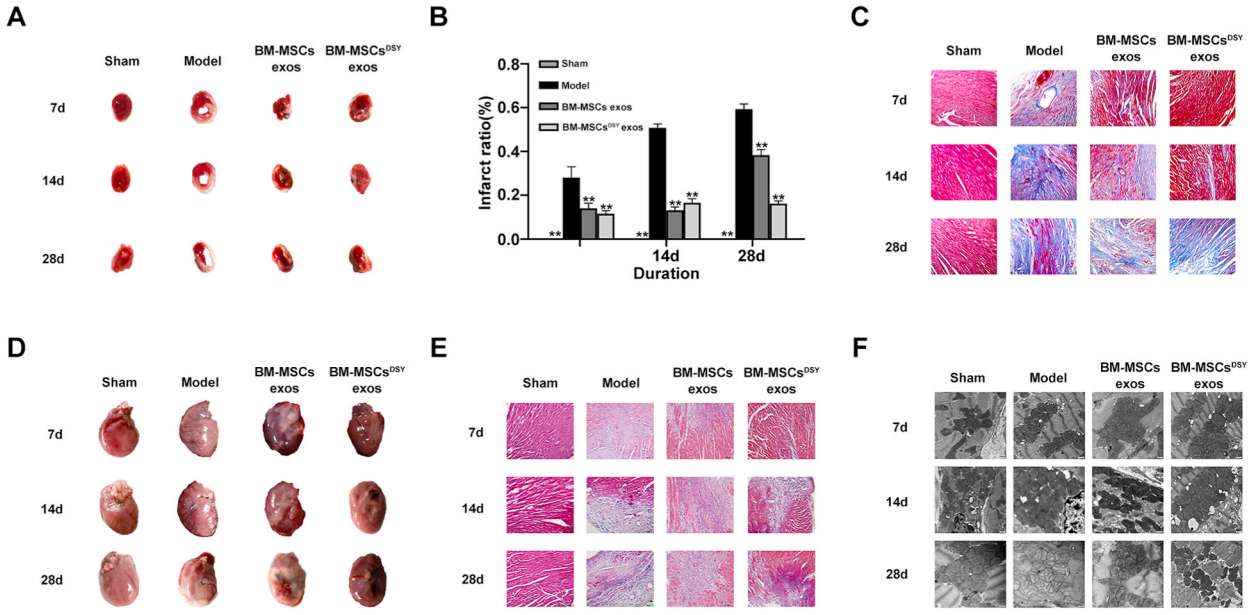

Fig. 3. Intramuscular injection of BM-MSCs^{DSY} exos can reduce infarction area and fibrosis, and can improve post-MI cardiac morphology, histopathology and cardiomyocyte ultrastructure A-B. TTC staining for infarction area on the 7th, 14th, and 28th days after MI; C. Representative MASSON staining for collagen on the 7th, 14th, and 28th days after MI (× 200); D. Cardiac morphology on the 7th, 14th, and 28th days after MI; E. Representative HE staining for cardiac histopathology on the 7th, 14th, and 28th days after MI (× 200); F. Representative cardiomyocytes' ultrastructure on the 7th, 14th, and 28th days after MI (× 25000). Data are presented as Mean ± SEM, n = 3, $^{**}P < 0.01$, $^{*}P < 0.05$.

cell infiltration was minimal. In the model group, myocardial fibers were slightly ruptured and some cardiomyocytes were swollen and deformed on the 7th day. This was followed by moderately disordered myocardial fiber arrangement, necrotic cardiomyocytes, and inflammatory cell infiltration on the 14th day, and extensive cardiomyocyte necrosis, dissolved myocardial fibers, numerous inflammatory cell infiltrations, and scar tissue formation on the 28th day. Compared to the model group, pathological changes were alleviated in both the BM-MSCs exos and BM-MSCs^{DSY} exos groups, with the latter showing less severe alterations. See Fig. 3E for details.

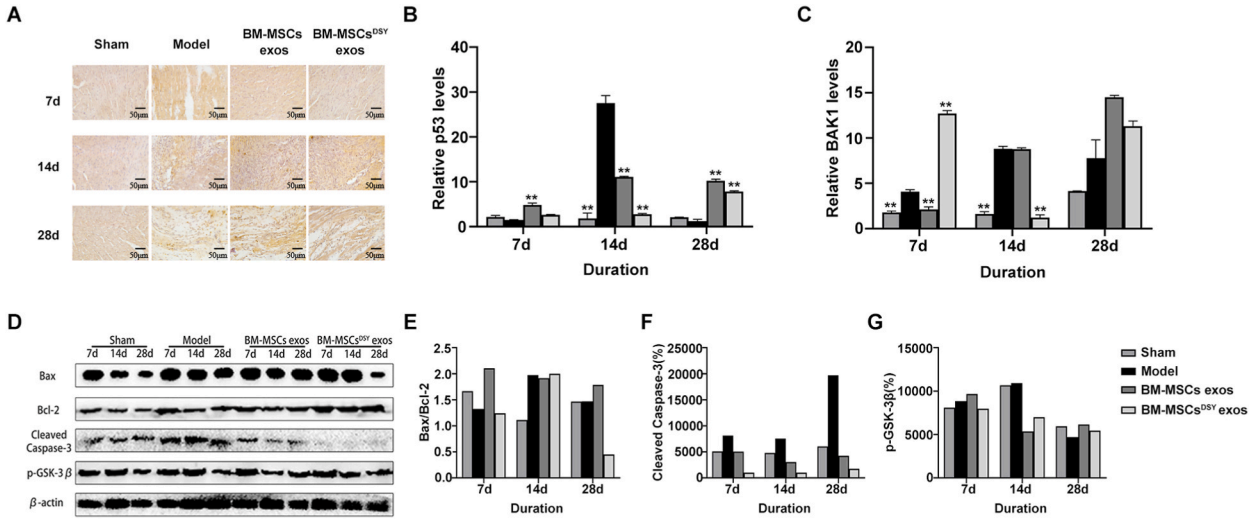

Fig. 4. Intramuscular injection of BM-MSCs^{DSY} exos inhibits post-MI cardiomyocyte apoptosis A. Representative TUNEL staining for apoptotic cardiomyocytes on the 7th, 14th, and 28th days after MI; B-C. Gene expression levels of *p53* and *BAK1* mRNA on the 7th, 14th, and 28th days after MI; D-G. Expression levels of the Bax/Bcl-2 ratio, Cleaved Caspase-3, and p-GSK-3β on the 7th, 14th, and 28th days after MI. Data are presented as Mean ± SEM, n = 3, $^{**}P < 0.01$, $^{*}P < 0.05$.

3.3.4. Ultrastructural changes of cardiomyocytes

In the sham group, regular-shaped mitochondria, dense and regular ridges, intact nuclear membranes, ordered myocardial fibers, and uniformly distributed filament lengths were observed. In the model group, swollen mitochondria, disordered ridges, ruptured nuclear membranes, and dissolved filaments were progressively aggravated with prolonged observation time. Compared to the model group, improvements were more noticeable in the BM-MSCs^{DSY} exos group than in the BM-MSCs exos group. See Fig. 3F for details.

3.4. BM-MSCs^{DSY} exos inhibited cardiomyocyte apoptosis

3.4.1. TUNEL staining results

As shown in Fig. 4A, only a few apoptotic cells were observed in the sham group, while the number of apoptotic cells gradually increased in the model group on the 7th, 14th, and 28th days. In comparison, apoptotic cardiomyocytes decreased in both the BM-MSCs exos and BM-MSCs^{DSY} exos groups.

3.4.2. Variation in gene expression of p53 and BAK1

Compared to the model group on day 7, the *p53* level was significantly higher ($P < 0.01$) in the BM-MSCs exos group, while the *BAK1* level was significantly lower ($P < 0.01$) in both the sham and BM-MSCs exos groups. In contrast, the levels of *p53* and *BAK1* were significantly elevated ($P < 0.01$) in the BM-MSCs^{DSY} exos group. On day 14, the levels of *p53* and *BAK1* were significantly decreased ($P < 0.01$) in all three groups. On day 28, the *p53* level increased and the *BAK1* level decreased in the sham group, while the levels of *p53* and *BAK1* were significantly higher ($P < 0.01$) in the BM-MSCs exos and BM-MSCs^{DSY} exos groups. See Fig. 4B–C for details.

3.4.3. Alterations in apoptosis-related protein expression

The expression levels of the Bax/Bcl-2 ratio, Cleaved Caspase-3, and p-GSK-3β were compared between the model group and the experimental groups on days 7, 14, and 28. See Fig. 4D–G for details.

The Bax/Bcl-2 ratio showed an increase in the BM-MSCs exos group and a decrease in the BM-MSCs^{DSY} exos group on days 7 and 28. However, no significant changes in the Bax/Bcl-2 ratio were observed in either group on day 14. Notably, the Bax/Bcl-2 ratio was consistently lower in the BM-MSCs^{DSY} exo group than in the BM-MSCs exos group at both 7 and 28 days.

The expression level of Cleaved Caspase-3 showed a decrease in both the BM-MSCs exos group and the BM-MSCs^{DSY} exo group, with lower expression levels observed in the latter group.

The expression level of p-GSK-3β also showed a decrease in both the BM-MSCs exos group and the BM-MSCs^{DSY} exo group on days 7 and 28. On day 28, the expression level of p-GSK-3β was lower than that on day 7 in all groups.

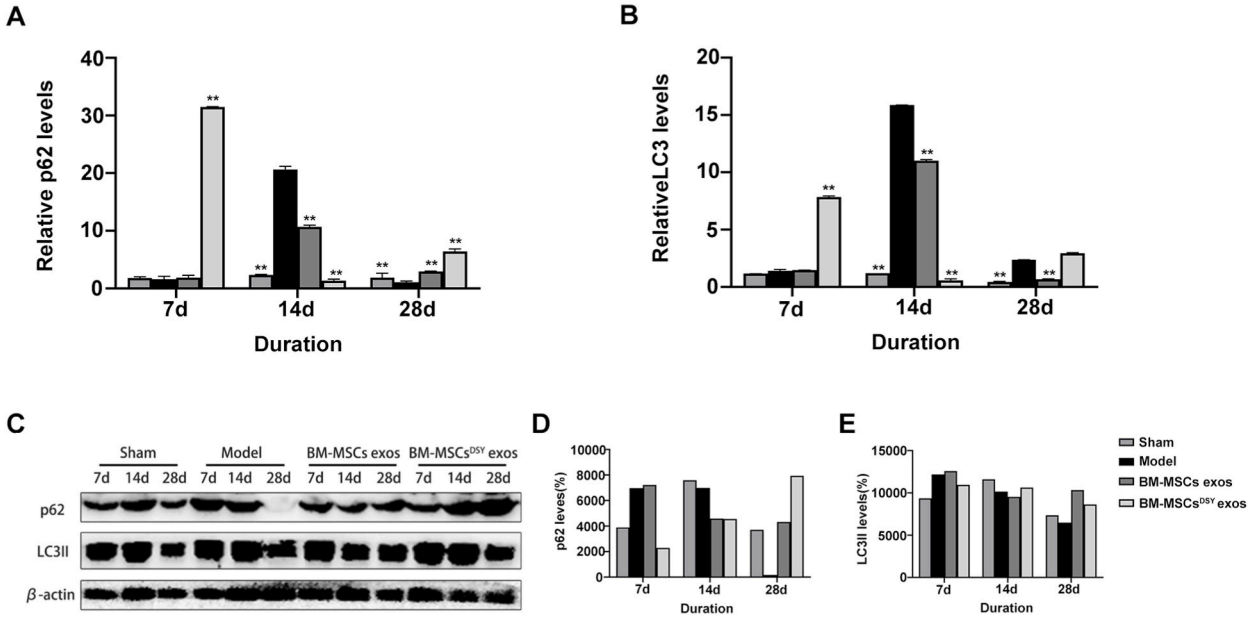

Fig. 5. Intramuscular injection of BM-MSCs^{DSY} exos promotes post-MI autophagy in myocardial cells A-B. Gene expression levels of *p62* and *LC3* mRNA on the 7th, 14th, and 28th days after MI; D-G. Expression levels of p62 and LC3II on the 7th, 14th, and 28th days after MI. Data are presented as Mean ± SEM, n = 3, $^{**}P < 0.01$, $^{*}P < 0.05$.

3.5. BM-MSCs^{DSY} exos increased autophagy levels in myocardial cells

3.5.1. Variation in gene expression of p62 and LC3

On day 7, the BM-MSCs^{DSY} exos group exhibited significantly higher levels of *p62* and *LC3* compared to the model group ($P < 0.01$). On day 14, the levels of *p62* and *LC3* had significantly decreased ($P < 0.01$) in the sham, BM-MSCs exos, and BM-MSCs^{DSY} exos groups. On day 28, all three groups displayed increased *p62* levels, but the BM-MSCs exos group showed a significantly lower *LC3* level ($P < 0.01$). Interestingly, the BM-MSCs^{DSY} exos group had higher *p62* and *LC3* levels than the BM-MSCs exos group on days 7 and 28, but lower levels on day 14. See Fig. 5A–B for details.

3.5.2. Changes in autophagy-related protein expression

The protein expression levels of p62 and LC3II were compared between the model and experimental groups on days 7, 14, and 28 (refer to Fig. 5C–E). On day 7, the BM-MSCs^{DSY} exos group showed a reduction in p62 expression, followed by a decline in both the BM-MSCs exos and BM-MSCs^{DSY} exos groups on day 14. By day 28, however, both groups exhibited increased p62 expression levels, with the BM-MSCs^{DSY} exos group having higher levels than the BM-MSCs exos group.

The expression level of LC3II in the BM-MSCs^{DSY} exos group decreased on day 7, while no significant changes were observed in the BM-MSCs exos and BM-MSCs^{DSY} exos groups on day 14. On day 28, both groups showed significantly increased LC3II expression levels. Notably, the BM-MSCs^{DSY} exos group had higher LC3II expression levels on days 7 and 28, but lower levels on day 14 compared to the BM-MSCs exos group.

4. Discussion

In this study, we found that: 1) BM-MSCs exos and BM-MSCs^{DSY} exos significantly decreased J-point elevation in electrocardiogram changes, increased serum myocardial zymogram activities, reduced myocardial infarct size and fibrosis, improved myocardial appearance and histopathological changes, and improved myocardiocyte ultrastructural damage over time; 2) Inhibition of cardiomyocyte apoptosis and induction of autophagy were responsible for the cardioprotective effect of BM-MSCs exos and BM-MSCs^{DSY} exos; 3) The caidiac protective effects of BM-MSCs^{DSY} exos were superior to those of BM-MSCs exos.

Massive cardiomyocyte necrosis and an intense inflammatory response resulted in deteriorated cardiac function, ventricular remodeling, heart failure and worse clinical outcomes after MI [13]. MSCs-based therapy has been recognized as a promising strategy for cardiac repair due to their favorable properties including easy isolation, multiple differentiation capacity and immunomodulatory properties [14]. Accumulative studies have revealed that the cardioprotective effects of MSCs are mainly attributed to their paracrine factors, especially small extracellular vesicles or exosomes [15]. MSCs exosomes-based therapies exert their cardioprotective effect through transferring endogenous molecules including lncRNA, miRNAs, and proteins to regulate cardiomyocyte apoptosis, angiogenesis, inflammatory reaction and myocardial fibrosis. Therefore, modification of MSCs exosomes to alter their molecular components is a bright strategy to augment their cardioprotective effects. To optimize MSCs exosomes, environmental stimuli are more feasible in clinical translation compared to genetic modification [16]. Deduction from the above proof, MSCs pretreated with drugs seem to be a solution to enhance cardiac repair effects in AMI treatment. Danshen decoction, a TCM prescription, has been shown to have numerous pharmacological actions in MI therapy, including anti-inflammatory, antioxidant, and anti-apoptotic properties. Our findings have demonstrated that MSCs exosomes pretreated with Danshen decoction exhibited superior cardioprotective effects in repair of the infarcted heart in MI rats.

Myocardial inflammation and fibroblasts play vital roles in cardiac repair after AMI; however, excessive inflammation and fibrosis might lead to catastrophic consequences, such as further loss of cardiomyocytes and then impairment of systolic function, ventricular remodeling, matrix degradation or even cardiac rupture [17]. Hence, proper and timely inhibitions of inflammation and fibrosis are essential in AMI therapy. Using a rat MI model, intramyocardial injection of BM-MSCs^{DSY} exos were beneficial in reducing infarct size on the 14th day and in suppressing inflammation and fibrosis on the 7th day.

Mitochondria have vital roles in cell metabolism such as ATP production, reactive oxygen species (ROS) generation, Ca^{2+} homeostasis modulation, and cell death control [18]. In normal cells, the inner mitochondrial membrane is highly impermeable to metabolites and ions. However, increased ROS production and Ca^{2+} overload following MI can cause the opening of mitochondrial permeability transition pore (mPTP), which results in the loss of mitochondrial inner membrane potential, uncoupling of the respiratory chain and a consequent drop of mitochondrial ATP synthesis. Increased permeability of the inner mitochondrial membrane ultimately leads to mitochondrial swelling, rupture and cardiomyocyte necrosis [19]. In our study, transmission electron microscopy (TEM) detection revealed that BM-MSCs^{DSY} exos could alleviate mitochondrial matrix swelling and mitochondrial membrane rupture from the 7th day.

In MI, myocardial apoptosis is the main cause of cardiomyocyte loss and plays a critical role in the incidence of myocardial dysfunction, ventricular remodeling, and even heart failure [20]. Apoptosis is regulated by two major pathways, intrinsic pathway activated by mitochondrial signaling and extrinsic pathway mediated by the binding of death ligands to death receptors on the cell surface. The intrinsic pathway is tightly regulated by the pro-apoptotic proteins (Bax and Bak), the anti-apoptotic proteins [B cell lymphoma 2 (Bcl-2), B cell lymphoma-extra-large (Bcl-xL), and myeloid cell leukemia-1 (Mcl-1)], and the Bcl-2 homology domain 3 (BH3)-only proteins (Bid, Bim, Noxa, and Puma). In MI, cellular stress activate p53 and BH3 only proteins, which in turn induces Bak/Bax oligomerization and permeabilization of the mitochondria, and ultimately promotes the release of cytochrome C (Cyt-C). The interaction between Cyt-C, apoptotic protease activating factor 1 (Apaf-1), and caspase-9 forms a multimeric complex called the apoptosome, which in turn activates caspase-9 and caspase-3, thereby eliciting apoptosis [21]. In addition, the activation of

caspase-dependent cell death pathways may also induce responses unrelated to apoptosis, such as cardiomyocyte hypertrophy [22].

Autophagy, originally defined as the delivery of cytoplasmic cargo to the lysosome for degradation, plays a crucial role in cellular physiology, including adaptation to metabolic stress, clearance of dangerous cargo, renovation during differentiation and development, and prevention of genomic damage. Canonical autophagy is a multiphasic process that involves the sequential and selective recruitment of autophagy related (ATG) proteins. Following, the expansion of phagophores is promoted by two distinct ubiquitin-like conjugation modules: one relies on the activity of ATG7 and ATG10 and enables the buildup of a multiprotein complex composed of ATG5, ATG12 and ATG16L1; the other involves ATG3, ATG4, and ATG7 and is ultimately responsible for the cleavage of members of the Atg8-family proteins, including mammalian microtubule-associated protein 1 light chain 3 (MAP1LC3/LC3) and their conjugation to phosphatidylethanolamine (PE). Among them, LC3 is most abundant in autophagosomal membranes and is well established as a marker to monitor the autophagosome and autophagic activity. Sequestosome 1 (SQSTM1/p62) recruit the ubiquitinated cargo to the autophagosomes by interacting with ubiquitinated proteins via its ubiquitin-associated domain and Lipidated LC3 (LC3-II) with its LC3-interacting region (LIR) [23]. Accumulated investigations have suggested important roles for autophagy in protection of cardiomyocytes from death following MI [24–26]. AMPactivated protein kinase (AMPK)-dependent autophagy protects cardiomyocytes against ischaemic injury by supplying energy metabolism substrate, which is consistent with the adaptive role of the autophagic response in conditions where availability of nutrients and oxygen supply are limited [27].

In addition to the well-known roles of p53 in regulating cell cycle checkpoints, DNA damage and repair, and apoptosis, it can affect autophagy in several cell lines [28,29]. Knockdown of p53 by cardiac autophagy inhibitory factor (CAIF) inhibits autophagy in cardiomyocytes [30]. Glycogen synthase kinase-3 beta (GSK3β), a serine/threonine protein Kinase, contributes to multiple receptor-mediated intracellular processes such as cell metabolism, gene expression, differentiation, migration, apoptotic death, and survival. The inactivation of GSK3β promotes cell survival by increasing the mPTP opening threshold and inhibiting proapoptic signals [31]. What's more, GSK3β serves a central signaling role in many regulatory processes through intersection with the PI3K, mTOR, PKB/AKT, WNT, and MAPK pathways [32]. Phosphorylated GSK3β exhibited pronounced positive effects on cardiomyocyte proliferation, autophagy promotion and angiogenesis following MI [33].

In the current study, the gene expressions of *p53*, *BAK1*, *p62*, and *LC3*, as well as the protein expressions of the Bax/Bcl-2 ratio, Cleaved Caspase-3, p-GSK-3β, p62, and LC3II, were used to measure variations in apoptosis and autophagy. These variations were observed in different groups: the model group, the BM-MSCs exos group, and the BM-MSCs^{DSY} exos group. On the 7th day, both apoptosis and autophagy levels increased in the model group and the BM-MSCs exos group, while they decreased in the BM-MSCs^{DSY} exos group. On the 14th day, both apoptosis and autophagy levels increased in the model group, while they decreased in the BM-MSCs exos group and the BM-MSCs^{DSY} exos group. On the 28th day, apoptosis level increased and autophagy level decreased in the model group, while apoptosis level decreased and autophagy level increased in the BM-MSCs exos group and the BM-MSCs^{DSY} exos group. It is worth noting that the gene expression level of *LC3* on the 7th day indicated an upregulation of autophagy. Additionally, the level of apoptosis was lower in the BM-MSCs^{DSY} exos group compared to the BM-MSCs exos group on the 28th day.

Nonetheless, several limitations of our findings should be highlighted. First, only one dose of MSCs-exos was adopted. Whether the beneficial effects of MSCs-exos are dose-dependent remains to be determined. Second, the principal bioactive components in BM-MSCs^{DSY} exos alleviating MI remains unclear. Further studies are required to detect the miRNA, mRNA, and protein profiles and to clarify the underlying mechanisms. Third, DSY is involved in inhibition of inflammatory and fibrotic responses to prevent the progression to heart failure following MI. Further studies need to be conducted to determine whether BM-MSCs^{DSY} exos have beneficial effects on these responses.

In summary, we demonstrated that BM-MSCs^{DSY} exos are superior to BM-MSCs-exos in improvement of cardiac function, morphology, histopathology and cardiomyocyte ultrastructure, as well as in reduction of infarction area and cardiac fibrosis by inhibiting apoptosis and promoting autophagy of cardiomyocytes following MI. Although our research is still in the laboratory, it has shed light on a promising cell-free therapeutic strategy of BM-MSCs^{DSY} exos for clinical treatment of MI.

Funding

This work was supported by the Natural Science Foundation of Shanxi province (Grant number 201901D211525), and the Scientific Research Project of Shanxi Traditional Chinese Medicine Administration (Grant number 2022ZYYC014).

Data availability statement

Data will be made available on request.

CRediT authorship contribution statement

Qian Yang: Writing – original draft, Funding acquisition, Formal analysis, Conceptualization. **Qi-Ming Zhong:** Software, Methodology. **Mei-qing Song:** Methodology, Investigation. **Li-guo Tong:** Methodology. **Chong-zhi Bai:** Writing – review & editing.

Declaration of competing interest

The authors declare that they have no known competing financial interests or personal relationships that could have appeared to influence the work reported in this paper.

Appendix A. Supplementary data

Supplementary data to this article can be found online at https://doi.org/10.1016/j.heliyon.2024.e38034.

References

[1] J. Chen, Y. Yang, C. Dai, Y. Wang, R. Zeng, Q. Liu, Serum cystatin C is associated with the prognosis in acute myocardial infarction patients after coronary revascularization: a systematic review and meta-analysis, BMC Cardiovasc. Disord. 22 (2022) 156, https://doi.org/10.1186/s12872-022-02599-5.
[2] X. Tong, J. Chen, W. Liu, H. Liang, H. Zhu, LncRNA LSINCT5/miR-222 regulates myocardial ischemia-reperfusion injury through PI3K/AKT pathway, J. Thromb. Thrombolysis 52 (2021) 720–729, https://doi.org/10.1007/s11239-021-02506-3.
[3] X. Fei, Y. Cai, F. Lin, Y. Huang, T. Liu, Y. Liu, Amniotic fluid mesenchymal stem cells repair mouse corneal cold injury by promoting mRNA N4-acetylcytidine modification and ETV4/JUN/CCND2 signal axis activation, Hum. Cell 34 (2021) 86–98, https://doi.org/10.1007/s13577-020-00442-7.
[4] R. Liu, W. Chang, H. Wei, K. Zhang, Comparison of the biological characteristics of mesenchymal stem cells derived from bone marrow and skin, Stem Cell. Int. 2016 (2016) 3658798, https://doi.org/10.1155/2016/3658798.
[5] A. Momeni, L. Eagler, C.Y. Lo, B.R. Weil, J.M. Canty Jr., J.K. Lang, S. Neelamegham, Neutrophils aid cellular therapeutics by enhancing glycoengineered stem cell recruitment and retention at sites of inflammation, Biomaterials 276 (2021) 121048, https://doi.org/10.1016/j.biomaterials.2021.121048.
[6] M. Devetzi, M. Goulielmaki, N. Khoury, D.A. Spandidos, G. Sotiropoulou, I. Christodoulou, V. Zoumpourlis, Genetically-modified stem cells in treatment of human diseases: tissue kallikrein (KLK1)-based targeted therapy, Int. J. Mol. Med. 41 (2018) 1177–1186, https://doi.org/10.3892/ijmm.2018.3361.
[7] A. Scafa Udriste, A.G. Niculescu, L. Iliuta, T. Bajeu, A. Georgescu, A.M. Grumezescu, E. Badila, Progress in biomaterials for cardiac tissue engineering and regeneration, Polymers 15 (2023) 1177, https://doi.org/10.3390/polym15051177.
[8] G. Schepici, S. Silvestro, E. Mazzon, Regenerative effects of exosomes-derived MSCs: an overview on spinal cord injury experimental studies, Biomedicines 11 (2023) 201, https://doi.org/10.3390/biomedicines11010201.
[9] S. Zhong, Y. Yin, Regulatory role of the programmed cell death 1 signaling pathway in sepsis induced immunosuppression, Front. Immunol. 14 (2023) 1183542, https://doi.org/10.3389/fimmu.2023.1183542.
[10] K. Valencia, L.M. Montuenga, Exosomes in liquid biopsy: the nanometric world in the pursuit of precision oncology, Cancers 13 (2021) 2147, https://doi.org/10.3390/cancers13092147.
[11] R. Kalluri, V.S. LeBleu, The biology, function, and biomedical applications of exosomes, Science 367 (2020) eaau6977, https://doi.org/10.1126/science.aau6977.
[12] M. Liu, G. Yuan, G. Luo, X. Guo, M. Chen, H. Yang, F. He, T. Yang, X. Zhang, Q. Wu, H. Zhou, S. Yang, Network pharmacology analysis and experimental verification strategies reveal the action mechanism of danshen decoction in treating ischemic cardiomyopathy, Evid Based Complement Alternat Med (2022) 7578055, https://doi.org/10.1155/2022/7578055, 2022.
[13] Y. Xiong, R. Tang, J. Xu, W. Jiang, Z. Gong, L. Zhang, Y. Ning, P. Huang, J. Xu, G. Chen, X. Li, M. Hu, J. Xu, C. Wu, C. Jin, X. Li, H. Qian, Y. Yang, Tongxinluo-pretreated mesenchymal stem cells facilitate cardiac repair via exosomal transfer of miR-146a-5p targeting IRAK1/NF-kappaB p65 pathway, Stem Cell Res. Ther. 13 (2022) 289, https://doi.org/10.1186/s13287-022-02969-y.
[14] H. Zheng, X. Liang, Q. Han, Z. Shao, Y. Zhang, L. Shi, Y. Hong, W. Li, C. Mai, Q. Mo, Q. Fu, X. Ma, F. Lin, M. Li, B. Hu, X. Li, Y. Zhang, Hemin enhances the cardioprotective effects of mesenchymal stem cell-derived exosomes against infarction via amelioration of cardiomyocyte senescence, J. Nanobiotechnol. 19 (2021) 332, https://doi.org/10.1186/s12951-021-01077-y.
[15] Y. Zou, L. Liao, J. Dai, M. Mazhar, G. Yang, H. Wang, N. Dechsupa, L. Wang, Mesenchymal stem cell-derived extracellular vesicles/exosome: a promising therapeutic strategy for intracerebral hemorrhage, Regen Ther 22 (2023) 181–190, https://doi.org/10.1016/j.reth.2023.01.006.
[16] H. Wu, Z. Peng, Y. Xu, Z. Sheng, Y. Liu, Y. Liao, Y. Wang, Y. Wen, J. Yi, C. Xie, X. Chen, J. Hu, B. Yan, H. Wang, X. Yao, W. Fu, H. Ouyang, Engineered adipose-derived stem cells with IGF-1-modified mRNA ameliorates osteoarthritis development, Stem Cell Res. Ther. 13 (2022) 19, https://doi.org/10.1186/s13287-021-02695-x.
[17] N.G. Frangogiannis, The inflammatory response in myocardial injury, repair, and remodelling, Nat. Rev. Cardiol. 11 (2014) 255–265, https://doi.org/10.1038/nrcardio.2014.28.
[18] Y. Zhang, J. Yao, M. Zhang, Y. Wang, X. Shi, Mitochondria-associated endoplasmic reticulum membranes (MAMs): possible therapeutic targets in heart failure, Front Cardiovasc Med 10 (2023) 1083935, https://doi.org/10.3389/fcvm.2023.1083935.
[19] N.G. Frangogiannis, Pathophysiology of myocardial infarction, Compr. Physiol. 5 (2015) 1841–1875, https://doi.org/10.1002/cphy.c150006.
[20] E. Teringova, P. Tousek, Apoptosis in ischemic heart disease, J. Transl. Med. 15 (2017) 87, https://doi.org/10.1186/s12967-017-1191-y.
[21] R. Qin, F.M. You, Q. Zhao, X. Xie, C. Peng, G. Zhan, B. Han, Naturally derived indole alkaloids targeting regulated cell death (RCD) for cancer therapy: from molecular mechanisms to potential therapeutic targets, J. Hematol. Oncol. 15 (2022) 133, https://doi.org/10.1186/s13045-022-01350-z.
[22] C. Putinski, M. Abdul-Ghani, R. Stiles, S. Brunette, S.A. Dick, P. Fernando, L.A. Megeney, Intrinsic-mediated caspase activation is essential for cardiomyocyte hypertrophy, Proc. Natl. Acad. Sci. U.S.A. 110 (2013) E4079–E4087, https://doi.org/10.1073/pnas.1315587110.
[23] B. Levine, G. Kroemer, Biological functions of autophagy genes: a disease perspective, Cell 176 (2019) 11–42, https://doi.org/10.1016/j.cell.2018.09.048.
[24] D. Wang, L. Lv, Y. Xu, K. Jiang, F. Chen, J. Qian, M. Chen, G. Liu, Y. Xiang, Cardioprotection of Panax Notoginseng saponins against acute myocardial infarction and heart failure through inducing autophagy, Biomed. Pharmacother. 136 (2021) 111287, https://doi.org/10.1016/j.biopha.2021.111287.
[25] K. Wang, Z. Li, Y. Li, X. Liu, Y. Sun, J. Hong, Y. Ding, W. Zheng, L. Qian, D. Xu, Cardioprotection of Klotho against myocardial infarction-induced heart failure through inducing autophagy, Mech. Ageing Dev. 207 (2022) 111714, https://doi.org/10.1016/j.mad.2022.111714.
[26] X. Zhang, Q. Wang, X. Wang, X. Chen, M. Shao, Q. Zhang, D. Guo, Y. Wu, C. Li, W. Wang, Y. Wang, Tanshinone IIA protects against heart failure post-myocardial infarction via AMPKs/mTOR-dependent autophagy pathway, Biomed. Pharmacother. 112 (2019) 108599, https://doi.org/10.1016/j.biopha.2019.108599.
[27] Y. Matsui, H. Takagi, X. Qu, M. Abdellatif, H. Sakoda, T. Asano, B. Levine, J. Sadoshima, Distinct roles of autophagy in the heart during ischemia and reperfusion: roles of AMP-activated protein kinase and Beclin 1 in mediating autophagy, Circ. Res. 100 (2007) 914–922, https://doi.org/10.1161/01.RES.0000261924.76669.36.
[28] S.S. Foster, S. De, L.K. Johnson, J.H. Petrini, T.H. Stracker, Cell cycle- and DNA repair pathway-specific effects of apoptosis on tumor suppression, Proc. Natl. Acad. Sci. U.S.A. 109 (2012) 9953–9958, https://doi.org/10.1073/pnas.1120476109.
[29] E. Tasdemir, M.C. Maiuri, L. Galluzzi, I. Vitale, M. Djavaheri-Mergny, M. D'Amelio, A. Criollo, E. Morselli, C. Zhu, F. Harper, U. Nannmark, C. Samara, P. Pinton, J.M. Vicencio, R. Carnuccio, U.M. Moll, F. Madeo, P. Paterlini-Brechot, R. Rizzuto, G. Szabadkai, G. Pierron, K. Blomgren, N. Tavernarakis, P. Codogno, F. Cecconi, G. Kroemer, Regulation of autophagy by cytoplasmic p53, Nat. Cell Biol. 10 (2008) 676–687, https://doi.org/10.1038/ncb1730.
[30] C.Y. Liu, Y.H. Zhang, R.B. Li, L.Y. Zhou, T. An, R.C. Zhang, M. Zhai, Y. Huang, K.W. Yan, Y.H. Dong, M. Ponnusamy, C. Shan, S. Xu, Q. Wang, Y.H. Zhang, J. Zhang, K. Wang, LncRNA CAIF inhibits autophagy and attenuates myocardial infarction by blocking p53-mediated myocardin transcription, Nat. Commun. 9 (2018) 29, https://doi.org/10.1038/s41467-017-02280-y.
[31] S. Ghaderi, N. Alidadiani, N. Dilaver, H.R. Heidari, R. Parvizi, R. Rahbarghazi, J. Soleimani-Rad, B. Baradaran, Role of glycogen synthase kinase following myocardial infarction and ischemia-reperfusion, Apoptosis 22 (2017) 887–897, https://doi.org/10.1007/s10495-017-1376-0.
[32] P. Cohen, S. Frame, The renaissance of GSK3, Nat. Rev. Mol. Cell Biol. 2 (2001) 769–776, https://doi.org/10.1038/35096075.
[33] Z. Yang, Y. Wu, L. Wang, P. Qiu, W. Zha, W. Yu, Prokineticin 2 (PK2) rescues cardiomyocytes from high glucose/high palmitic acid-induced damage by regulating the AKT/GSK3beta pathway in vitro, Oxid. Med. Cell. Longev. (2020) 3163629, https://doi.org/10.1155/2020/3163629, 2020.